Petroleum Science (2021) 18:295–306
https://doi.org/10.1007/s12182-020-00531-0

ORIGINAL PAPER

Synthesis of highly active Cu(I)-Y(III)-Y zeolite and its selective adsorption desulfurization performance in presence of xylene isomers

Bo-Long Jiang[1] · Nan Jiang[1] · You-Xin Chang[2]

Received: 22 May 2020 / Accepted: 7 September 2020 / Published online: 1 December 2020

Abstract

Abstract A bimetal-exchanged NaY zeolite (Cu(I)-Y(III)-Y) with a desirable adsorptive desulfurization (ADS) performance was prepared and characterized by means of X-ray diffraction, specific surface area measurements, X-ray fluorescence spectrometer, X-ray photoelectron spectroscopy, thermal gravity analysis and Fourier transform infrared spectroscopy. The effect of Y(III) ions on ADS in the presence of the xylenes was investigated. Results indicated that the ADS performance of Y(III)-Y is higher than that of most reported CeY. The Y(III)-based Cu(I)-Y(III)-Y demonstrated the higher breakthrough loading than those of reported Ce(III)/Ce(IV)-based transition metal Y zeolites, showing that Y(III) ions play a promoting role in improving the ADS selectivity. For Cu(I)-Y(III)-Y, a new strong S-M interaction (S stands for sulfur, while M stands for metal) active site was formed, which might be caused by the synergistic effect between Cu(I) and Y(III). The Cu(I)-Y(III)-Y, which combined the advantages of Cu(I)-Y and Y(III)-Y, is a kind of promising adsorbent. The breakthrough loading decreased in the order of Cu(I)-Y(III)-Y > Y(III)-Y > Cu(I)-Y, and the effect of xylene isomers on the sulfur removal was in the order of ortho-xylene > meta-xylene > para-xylene, which exhibited the same trend with the bond order of xylenes.

Keywords Desulfurization · Yttrium · Copper · Y zeolite · Competitive adsorption · Xylenes

1 Introduction

As environmental awareness grows, deep and ultra-deep removal of sulfur from fuel has become an important global issue (Wang et al. 2019). Hydrodesulfurization (HDS) is currently the most common desulfurization method used in the industry (Li et al. 2020). However, to achieve deep desulfurization, HDS needs to utilize very severe conditions because aromatic sulfur compounds, such as thiophene and its derivatives, are particularly difficult to treat by conventional HDS. Adsorptive desulfurization (ADS) is considered to be an efficient and economic technology for the selective removal of thiophene and its derivatives because of its particular advantages, such as operating under mild conditions, not changing the performance of oil products and environmental friendliness (Subhan et al. 2018a, b; Li et al. 2017; Zu et al. 2020).

Y zeolites with well-defined three-dimensional channels with a large pore opening of 7.4 Å × 7.4 Å and a supercage cavity of 11.0 Å × 13.0 Å have been widely investigated (Kolev et al. 2010). Because of their special three-dimensional channels and a large amount of cation-exchangeable sites, ion-exchanged Y zeolites generally possess a higher adsorption capacity than other zeolites (Isoda et al. 2000). Many researchers reported that transition metal Cu(I), Cu(II), Ag(I), Ni(II) and Zn(II) ion-exchanged NaY zeolites are effective adsorbents for the selective removal of thiophene (TP) and its derivatives (Li et al. 2020; Oliveir et al. 2009). Among these adsorbents, the Cu(I)-Y shows the highest adsorptive sulfur capacity (Hernández-Maldonado et al. 2005; Hernández-Maldonado and Yang 2003). However, the desulfurization capability of Cu(I)-Y can be strongly affected

Edited by Xiu-Qiu Peng

Electronic supplementary material The online version of this article (https://doi.org/10.1007/s12182-020-00531-0) contains supplementary material, which is available to authorized users.

✉ Bo-Long Jiang
jiangbolong@qut.edu.cn

[1] Innovation Institute for Sustainable Maritime Architecture Research and Technology, Qingdao University of Technology, Qingdao 266000, China

[2] Chongqing Changshou Sino French Water Co. Ltd., Chongqing 404100, China

by the competitors, such as aromatics, through π-electron interaction (Bhandari et al. 2006).

Rare-earth elements exhibit excellent physical, chemical, optical and electrical properties because they have unfilled 4f electrons (Song et al. 2015; Wang et al. 2016). To improve the competitive adsorption, rare earth metal S–M (S stands for sulfur, while M stands for metal) adsorbents have received a great deal of attentions. Shi et al. (2013) found that the LaNaY exhibited high ADS selectivity in the presence of cyclohexene. The Brönsted acid sites play an important role in the removal of thiophene from model gasoline-containing olefin (Li et al. 2017). Among metal ion-exchanged Y zeolites, the CeY zeolite has been greatly studied owing to its high adsorption selectivity to sulfur compounds when aromatics exist (Velu et al. 2003; Subhan et al. 2018a). Unfortunately, the application of rare earth metal-exchanged zeolites is limited because of their low ADS capacities (Wang et al. 2009; Qin et al. 2014a, b). Therefore, the combination of transition metal sites, which possess the high sulfur capacities, with rare earth metal sites would endow the promising adsorbents for ADS. To overcome the aforementioned problem, Song et al. (2013, 2014) reported that the Cu(I)Ce(IV)Y and Ag(I)Ce(IV)Y adsorbents, which possessed both high ADS capacity similar to Cu(I)Y and Ag(I)Y and high selectivity to sulfur compounds similar to Ce(IV)Y in presence of competitors, such as toluene and so on. Recently, it was found that the valence state of cerium in CeY greatly affects thiophene (TP) adsorption capacity (Liao et al. 2015). Replacing Ce(IV) by Ce(III) in CeY is favorable for improving the adsorption capacity of TP but not benzene adsorption capacity. Unfortunately, the Ce(III) is the most easily converted to Ce(IV) among the lanthanides, therefore it is difficult to control the valence state of cerium during the high temperature calcination, which is needed to eliminate the impurities and endow high surface area. The common valence of rare-earth yttrium (Y) is trivalent. In addition, the Y(III) ions is stable and therefore can keep its trivalent state during high temperature calcination. However, the yttrium-exchanged zeolites have not been studied yet. In this study, the Cu(I)-Y, Y(III)-Y and Cu(I)-Y(III)-Y were synthesized. The effect of Y(III) ions on selective ADS in the presence of the xylene isomers was investigated. The aim of this study is to develop a type of highly active ADS adsorbent based on yttrium. For this purpose, we have compared the active sites of as-prepared adsorbents and explored the reasons for the enhanced ADS selectivity of yttrium-based zeolites in presence of xylenes by the theoretical analysis. As expect, the Y(III)-Y showed higher ADS breakthrough loadings than that of reported CeY zeolites for model oils with and without aromatic competitors. The Cu(I)-Y(III)-Y, which combined the advantages of the Cu(I)Y and Y(III)Y, showed the highest breakthrough loadings for the model oils containing xylene isomers, and the breakthrough loading decreased in the order of Cu(I)-Y(III)-Y > Y(III)-Y > Cu(I)-Y. The Y(III) ions in the zeolites play a promoting role in improving the selectivity to sulfur.

2 Experimental

2.1 Model oil sample

The TP and benzothiophene (BT) were dissolved into *n*-octane solvent, respectively, to make model oils of M1 and M2. The aromatic competitors o-xylene, m-xylene and p-xylene were dissolved into *n*-octane solvent containing TP, respectively, to make model oils of M3, M4 and M5, and dissolved into *n*-octane solvent containing BT, respectively, to make model oils M6, M7 and M8. Sulfur concentration of all the model oils is 200 mg L^{-1}, and the xylene concentration of M3 to M8 is 500 mg L^{-1} (See Table S1).

2.2 Adsorbents preparation

The Cu(I)-Y and Y(III)-Y adsorbents were prepared by treating the NaY (Si/Al = 2.86) with a 0.1 mol L^{-1} $Y(NO_3)_3$ and $Cu(NO_3)_2$ solution at room temperature for 48 h, respectively. After ion exchange, the solids were separated by filtration, and then dried at 110 °C for 12 h, calcined at 550 °C for 4 h to obtain the Y(III)-Y and Cu(II)-Y. Similarly, the Cu(II)-Y(III)-Y adsorbent was prepared by ion-exchanging the Y(III)-Y with 0.1 mol L^{-1} $Cu(NO_3)_2$ solution. Finally, the calcined Cu(II)-Y and Cu(II)-Y(III)-Y were reduced at 190 °C for 3 h under hydrogen atmosphere to obtain the Cu(I)-Y and Cu(I)-Y(III)-Y. To determine the best Cu/Y metal molar ratio the Cu(I)-Y(III)-Y samples with different Cu/Y metal molar ratios (x = 1/9, 1/5, 1/3, 1/2, 1/1, 2/1, 3/1, 5/1, 9/1) were also prepared by changing the concentration of the $Y(NO_3)_3$ and $Cu(NO_3)_2$ solutions.

2.3 Characterizations

The XRD analysis was carried out on a D/max-2200PC-X-ray diffractometer. The typical properties were analyzed by nitrogen adsorption and desorption using Micromeritics adsorption equipment of NOVA2000e. The XPS was conducted by PHI-1600 spectrometer with hemispherical analyzer and MgKα (1253.6 eV). The recorded photoelectron binding energies were referenced against the C 1 s contamination line at 284.8 eV. The chemical compositions were determined by Shimadzu XRF-1800 wavelength dispersive X-ray fluorescence spectrometer (XRF). TG-DTG analysis was performed on a DuPont 2100 (Perkin Elmer, America). Fourier transform infrared spectra (FT-IR and Py-FTIR) were obtained on a PE Spectrum GX FTIR spectrometer.

2.4 Adsorption experiments

Typically, 1.0 g adsorbent was placed in the center of the fixed-bed. The Cu(I) ions on surface of the Cu(I)-Y and Cu(I)-Y(III)-Y can be partly oxidized to Cu(II) ions when they are placed in the air. Therefore, prior to the each experiment, the Cu(I)-Y and Cu(I)-Y(III)-Y adsorbents were activated in flowing H_2 gas at 190 °C for 1 h (with H_2 flowrate of 100 mL min^{-1}) and then cooled down to the adsorption temperature. This is an essential step to obtain the Cu(I)-Y or Cu(I)-Y(III)-Y zeolites with high activity. The model oil was pumped into the fixed-bed at a flowrate of 0.26 mL/min, and effluents were collected at regular intervals. The sulfur content was determined by Shimadzu FPD-GC-14C gas chromatograph equipped with flame photometric detector and a capillary column (PH-1, 60 m × 0.25 mm).

For static adsorption, 0.2 g of adsorbent was added to a round-bottom flask containing 20 mL model oil, which was then placed in a water bath equipped with a condenser pipe at 50 °C and held for 1 h under magnetic stirring, and the supernatant liquor was analyzed.

3 Results

3.1 Adsorbent characterization

3.1.1 XRD and SEM

The XRD patterns of the NaY and Cu(I)-Y (b), Y(III)-Y (c) and Cu(I)-Y(III)-Y zeolites are presented in Fig. 1. The similarity of the XRD patterns of the Cu(I)-Y, Cu(I)-Y(III)-Y, Y(III)-Y to that of the original NaY indicates that the original zeolite structure remained unchanged. However, a slight decrease in the peak intensity after the exchange process was also found because of the introduction of metal ions. This indicates that the metal ion-exchange with the parent NaY caused a certain extent of reduction in crystallinity (Li et al. 2009). Additionally, no peaks of metal oxides were seen. The crystallinities of the zeolites determined from XRD results were listed in Table 1. The effect of yttrium on the crystallinity of zeolites was very serious than that of copper, which was possibly because the Y(III) ions were more easily ion-exchanged with NaY to give a higher Na(I) exchange degree in both Y(III)-Y and Cu(I)-Y(III)-Y (see Table 1). This will be further discussed in Sect. 3.1.3 XRF. In addition, the molecular diameter of Y is larger than that of Cu, therefore, Y(III) in zeolite would cause a great effect on crystallinity. The SEM results (Fig. S1) of Cu(I)-Y, Cu(I)-Y(III)-Y and Y(III)-Y showed that morphology of NaY was remained unchanged after ion-exchange, which in agreement with the XRD results.

3.1.2 BET

Table 1 shows the BET results of Cu(I)-Y (b), Y(III)-Y (c) and Cu(I)-Y(III)-Y adsorbents. The surface area (S_{BET}) and pore volume (V_p) of NaY were 642 m^2 g^{-1} and 0.361 cm^3 g^{-1}, respectively. After metal ion-exchange, the S_{BET} and V_p of all adsorbents decreased. This was possibly because of the presence of copper and yttrium particles in the network of NaY, which might block the channels of NaY. The S_{BET} and V_p decreased in the order of NaY > Cu(I)-Y > Y(III)-Y > Cu(I)-Y(III)-Y, which was consistent with the changing trend of zeolite crystallinity.

3.1.3 XRF

The chemical compositions of the NaY and Cu(I)-Y, Y(III)-Y and Cu(I)-Y(III)-Y zeolites were summarized in Table 1. Ion-exchange degrees (α) in Table 1 were calculated by the following equation (Mo et al. 2019):

$$\alpha = ([\mathrm{Na}(I)]_{\mathrm{NaY}} - [\mathrm{Na}(I)]_{\mathrm{zeolite}})/[\mathrm{Na}(I)]_{\mathrm{NaY}} \times 100 \quad (1)$$

where $[\mathrm{Na}(I)]_{\mathrm{NaY}}$ and $[\mathrm{Na}(I)]_{\mathrm{zeolite}}$ represents the number of Na(I) ions in Na(Y) and zeolites (Cu(I)-Y, Y(III)-Y or Cu(I)-Y(III)-Y), respectively. It can be seen in Table 1 that the ion-exchange degree of the Cu(I)-Y was only 74.4%, while the ion-exchange degree of Y(III)-Y was 79.6%, which is higher than that of Cu(I)-Y. For Cu(I)-Y(III)-Y, the total ion-exchange degree was 81.6%, among which 61.2% was contributed by Y(III) ions, and 20.1% was contributed by Cu(II) ions, indicating that Y(III) ions were easier to substitute Na(I) ions in NaY than Cu(II) ions. The higher ion-exchange degree of Y(III) compared to Cu(II) could be attributed to an effective interaction of Y(III) with the zeolite framework (Kim et al. 1994). This showed that the trivalent cation was

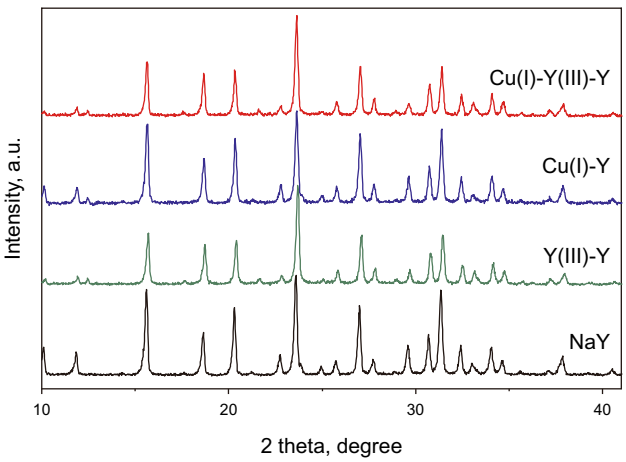

Fig. 1 XRD patterns of NaY and Cu(I)-Y, Y(III)-Y and Cu(I)-Y(III)-Y

Table 1 Chemical and physical properties of NaY and Cu(I)-Y, Y(III)-Y and Cu(I)-Y(III)-Y

Adsorbents	S_{BET}, $m^2\ g^{-1}$[a]	V_p, $cm^3\ g^{-1}$	r_p, nm	Crystallinity, %[b]	Si/Al mole ratio[c]	α, %[c]	Unit cell formula[c]
NaY	642	0.361	1.13	100	2.86	—	$Na_{49}Al_{49}Si_{140}O_{384}$
Cu(I)-Y	618	0.341	1.10	95.4	2.82	74.4	$Na_{13}Cu_{18}Al_{49}Si_{140}O_{384}$
Y(III)-Y	601	0.329	1.09	71.5	2.84	79.6	$Na_{10}Y_{13}Al_{49}Si_{140}O_{384}$
Cu(I)-Y(III)-Y	561	0.315	1.12	69.8	2.87	81.6	$Na_9Cu_5Y_{10}Al_{49}Si_{140}O_{384}$

[a]S_{BET} refers to BET surface area, V_p refers to pore volume and r_p refers to average pore diameter

[b]Obtained from XRD analysis

[c]Obtained by XRF analysis

more favorable for neutralizing the framework charge in Y zeolites (Velu et al. 2003), which led to the serious partial disruption of the crystalline structure (Thomas et al. 2010). This is also in agreement with the XRD and BET analysis.

3.1.4 XPS

The results of XPS spectra of Cu(I)-Y (b), Y(III)-Y (c) and Cu(I)-Y(III)-Y are shown in Fig. 2. It can be observed in Fig. 2a, for Cu(I)-Y, the peaks at 932.7 eV, and 952.6 eV can be attributed to the characteristic of Cu(I) species (Wang et al. 2019; Liu et al. 2014). While the small peak at 935.3 eV can be assigned to Cu(II) species, indicating that most of the Cu(II) was reduced to Cu(I). For Cu(I)-Y(III)-Y, the peaks of Cu(I) located at 932.3 eV and 952.3 eV, while the peak of Cu(II) located at 933.7 eV. All these peaks shifted to the lower binding energies, suggesting that the electronic environment of the Cu was changed due to transfer of some electrons from Y to Cu (Wang et al. 2016). This indicates that the Y(III) in Cu(I)-Y(III)-Y zeolite acts as an electron donor. As shown in Fig. 2b, for Y(III)-Y, the peaks at 153.5 and 160.4 eV can be seen, which are attributed to Y(III) species (Moulder et al. 1995). It can be confirmed that the Y(III) is stable and can keep its trivalent valence state after high temperature calcination, which is different from Ce(III). As compared to Y(III)-Y, the peaks of Y(III) species of Cu(I)-Y(III)-Y shifted to the higher values of 155.3 eV and 161.4 eV, confirming that the electronic environment of the Y(III) was changed by Cu(I), which agrees with the results observed for Cu 2p regions. Similar results were also obtained by Bondarenka (2001).

3.1.5 Py-FT-IR

The FT-IR spectra of pyridine adsorbed on Cu(I)-Y, Y(III)-Y and Cu(I)-Y(III)-Y at 50, 150 and 300 °C are shown in Fig. S2, and the Lewis and Brönsted acidity values were calculated according to the method of Emeis (1993), and the results are listed in Table 2. It is well known that the NaY zeolite exhibit only weak Lewis acidity originated in Na(I) ions. It can be seen from Table 2, after introduction of Cu and Y, Brönsted acid sites, and medium and strong Lewis acid sites were formed over Cu(I)-Y, Y(III)-Y and

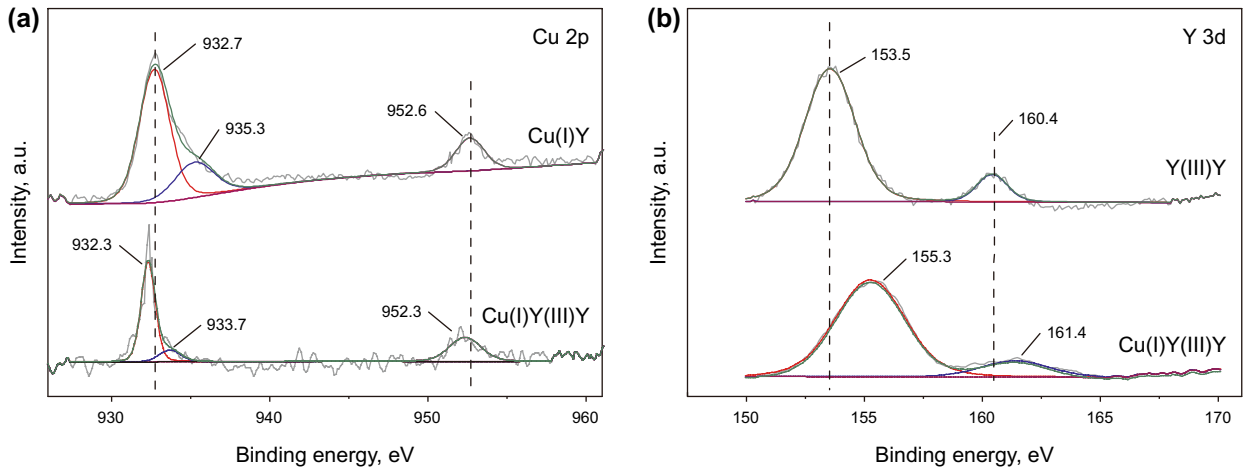

Fig. 2 XPS spectra of Cu 2p (**a**) and Y 3d (**b**) regions on the surface of Cu(I)-Y, Y(III)-Y and Cu(I)-Y(III)-Y

Cu(I)-Y(III)-Y. Lewis acid sites was formed because Cu(I) and Y(III) were existed as electron acceptor and could form –O–Cu and –O–Y structures on zeolites (Gupta and Paul 2014). Brönsted acid sites were generated due to the dissociation of water in the hydrated metal ions during calcination of metal ions-exchanged zeolites (Mo et al. 2019).

For Cu(I)-Y, the amount of Lewis acid sites was much more than that of the Brönsted acid sites for all the desorption temperatures, showing that the Lewis acid sites were predominant for Cu(I)-Y (Song et al. 2016; Wang et al. 2008). This observation is consistent with the reported results of Gong et al. (2009), who studied CuY and also found that Lewis acid sites were dominant. For Y(III)-Y, the amount of Brönsted acid sites were much higher than that of Cu(I)-Y for all the desorption temperatures, showing that Y(III)-Y could provide more Brönsted acid sites than Cu(I)-Y. Similar pyridine adsorption results on CuY (Song et al. 2013) and CeY (Song et al. 2016; Qin et al. 2014a; Zu et al. 2019a, b) have been obtained. It can also be observed that for Cu(I)-Y(III)-Y, the amount of Lewis acid site at all the desorption temperatures were higher than those of Y(III)-Y. As mentioned above, this is because Cu(I)-Y mainly provide Lewis acid sites, therefore addition of Cu(I) to Y(I)-Y can induce more Lewis acid sites. Similarly, the Cu(I)-Y(III)-Y possessed more Brönsted acid sites at all the desorption temperatures than those of Cu(I)-Y, which is because the Y(III)-Y can provide more Brönsted acid sites than that of Cu(I)-Y. Additionally, the amounts of Lewis acid site of Cu(I)-Y(III)-Y and Y(III)-Y decreased significantly with increasing desorption temperature from 150 to 300 °C, showing that the weak Lewis sites were predominant for these adsorbents (Gupta and Paul 2014).

3.2 Adsorptive desulfurization of model oil

3.2.1 ADS of model oil containing TP and BT

To determine the best Cu/Y metal molar ratio (x), the Cu(I)-Y(III)-Y adsorbents with different x were tested via static adsorption experiment with model oil M2 (Fig. S3). The results showed that with increasing x the ADS rate of Cu(I)-Y(III)-Y increases first, reaches a high value of 98.0% at $x = 1/1$, then tends to an equilibrium value. Therefore, the Cu(I)-Y(III)-Y with $x = 1/1$ was used in the rest of this studies. The breakthrough results for ADS over Cu(I)–Y, Y(III)–Y and Cu(I)–Y(III)–Y from M1 and M2 (only containing TP or BT) are presented in Fig. 3, Fig. S4 and Table S2. For M2, it can be seen that the Cu(I)-Y and Cu(I)-Y(III)-Y zeolites were found to be highly effective and showed a high capacity for BT removal with breakthrough loadings of 4.84 wt% and 2.92 wt%, respectively. In contrast, for Y(III)-Y, a much lower BT breakthrough loading of 2.00 wt% was found. This indicates that the addition of Cu in the Y zeolite plays an important role in improving the ADS capacity. Similar trends were also observed with M1 for TP removal onto these adsorbents. This is possibly because Cu(I)-Y(III)-Y possessed similar adsorption sites to Cu(I)-Y. This will be discussed in Sect. 4.1.1. It is well-known that Cu(I)-Y possessed the high ADS capacity because of the π-complexation between the sulfur compounds and the Cu(I) on the adsorbent. The amount of weak acid sites is also one of the important factors affecting ADS capacity (Yi et al. 2014). Additionally, for all the adsorbents, the breakthrough loading of BT was much higher than that of TP, which showed that the ADS selectivity decreases in the order of BT > TP. This is in agreement with the reported results (Wang et al. 2012).

Table 2 Distribution of Brönsted and Lewis acidity in Cu(I)-Y, Cu(I)-Y(III)-Y and Y(III)-Y

Sample	Desorption temperature, K	Brönsted acidity, μmol g^{-1}	Lewis acidity, μmol g^{-1}	Total acidity, μmol g^{-1}	Ratio of L/B
Cu(I)-Y	323	60.2	660.8	721.0	10.98
	423	43.1	264.9	308.0	6.15
	573	40.9	159.3	200.2	3.89
Cu(I)-Y(III)-Y	323	116.4	592.2	708.6	5.09
	423	105.1	221.4	326.5	2.11
	573	94.7	142.8	237.5	1.51
Y(III)-Y	323	157.2	474.3	631.5	3.02
	423	142.9	219.3	362.2	1.53
	573	127.5	51.7	179.2	0.41

3.2.2 Effect of xylene isomers on ADS

The breakthrough curves and declines in breakthrough loadings for ADS from M3, M4, M5 containing TP, and M6, M7, M8 containing BT were summarized in Fig. 3, Fig. S4 and Table S2. For all the fuel containing xylenes (M3 to M8), Cu(I)-Y(III)-Y showed the highest breakthrough loadings for both TP and BT among the as-prepared samples (Fig. 3, Table S2). This confirmed that the Y(III) ion in Cu(I)-Y(III)-Y-induced a high selectivity to sulfur, while the Cu(I) ion in Cu(I)-Y(III)-Y led to a high sulfur capacity. Therefore, the synergistic interaction between Cu(I) and Y(III) induced a high sulfur capacity for Cu(I)-Y(III)-Y. The breakthrough loadings for all the model oils decreased in the order of Cu(I)-Y(III)-Y > Y(III)-Y > Cu(I)-Y.

For M3 to M8 (Fig. 3, Table S2), a noticeable decreases in the breakthrough loading over all the absorbents were observed both for TP and BT comparing with those of corresponding M1 and M2 without xylene. The decline in breakthrough loading decreased in the order of Cu(I)-Y > Cu(I)-Y(III)-Y > Y(III)-Y. Upon the introduction of Y(III) ions to Cu(I)-Y, the decline in sulfur loading decreased both for TP and BT. This is because the strong S-M interaction between sulfur molecules with zeolites through Y(III) sites in Cu(I)-Y(III)-Y, which makes TP and BT adsorption relatively less affected by xylenes (Liu et al. 2014). In addition, the protonation of BT and TP due to the Brönsted acid sites play a role since the addition of Y(III) promotes formation of Brönsted acid sites, this is another reason for the improvement of selective ADS performance upon introduction of Y(III). However, the sulfur absorbed on the Cu(I) sites in Cu(I)-Y(III)-Y by the π-complexation would be affected by the existence of xylenes (similar to Cu(I)-Y). Therefore, the effect of xylenes on the ADS over Cu(I)-Y(III)-Y would be greater than that of Y(III)-Y.

For all the adsorbents (Table S2), the effect of the o-xylene was the most serious as compared to m-xylene and p-xylene. While the declines in breakthrough loadings of Cu(I)-Y(III)-Y (11.5% for TP and 9.3% for BT) and Y(III)-Y (10.9% for TP and 9.0% for BT) with M5 and M8 containing p-xylene were very low. The effects of the xylene isomers on BT and TP ADS were in the order of o-xylene > m-xylene > p-xylene. The reason for this will be further discussed in Sect. 4.2.

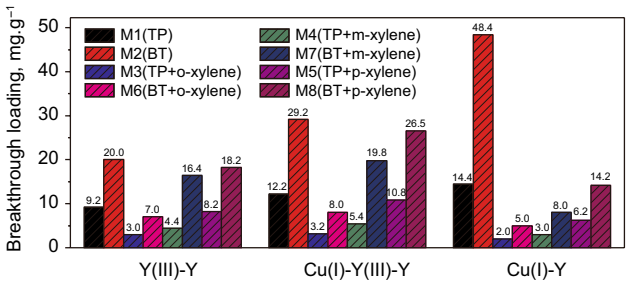

Fig. 3 Breakthrough loadings of TP for M1, M3, M4, M5 and BT for M2, M6, M7, M8 (Sulfur concentration of all the oils is 200 mg L^{-1}, and xylene concentration of each oils is 500 mg L^{-1}) over Cu(I)-Y (b), Y(III)-Y (c) and Cu(I)-Y(III)-Y

3.2.3 Comparison of breakthrough capacity of TP and BT

It is worthy to note that the sulfur breakthrough loadings of Y(III)-Y are higher than that of most reported CeY zeolites for model oils with and without aromatics (Table S3). In addition, similar results were also observed for the Cu(I)-Y(III)-Y, which demonstrating that the sulfur breakthrough loadings of Cu(I)-Y(III)-Y are higher than those of Cu(I)-Ce(IV)-Y and AgCeY. It should be noted that this comparison is not accurate since the ADS conditions, and the compositions of model oils are somewhat different. However, these results confirmed that Y(III)-Y possessed higher ADS breakthrough capacity than that of CeY, and the as-prepared Cu(I)-Y(III)-Y is highly active adsorbent for ADS.

4 Theoretical analysis and computer simulations

4.1 Theoretical analysis

4.1.1 Analysis of active sites

For better understanding of adsorption mode and adsorptive affinities of different zeolites with sulfur compounds, TP was chosen as the model sulfur compound. The TG-DTG patterns of zeolites before and after adsorbing TP are shown in Fig. 4. For all the samples, the loss of water occurred in the temperature range of 40–200 °C (Gabruś et al. 2015). Comparing with fresh Cu(I)-Y (Fig. 4a), a new strong weight loss peak at 339 °C with a very weak shoulder peak (378 °C) can be seen for spent Cu(I)-Y (Fig. 4b). The strong peak at 339 °C can be attributed to the loss of TP adsorbed on the Cu(I)-Y zeolite by π-complexation (Hernández-Maldonado and Yang 2003). For the Y(III)-Y and Cu(I)-Y(III)-Y, the peak at 378 °C can also be observed, showing that these three zeolites possessed at least a same kind of adsorption sites. The measurement of FT-IR spectra of TP adsorption on Ce(IV)Y confirmed the protonation of TP on Brönsted acid sites also plays an important role in ADS (Shi et al. 2012; Tarafdar et al. 2005). Thus, considering that all these three adsorbents possessed Brönsted acid sites (Sect. 3.1.5), and TP is alkali compounds, we attributed the peak to the loss of TP adsorbed via the protonation reaction, which

occurred as TP adsorbed onto as-prepared zeolites due to the Brönsted acid sites. This will be further discussed in Sect. 4.1.2 combined with the FT-IR analysis of the adsorbents after adsorbing model oil M1. For Y(III)-Y after adsorbing of TP (Fig. 4d), three weight loss peaks located at 378, 450 and 509 °C can be seen, showing that there are different adsorptive sites co-existing in Y(III)-Y. The former can be attributed to the protonation of TP, and the the latter two can be assigned to S-M interactions (Liu et al. 2014; Wang et al. 2020), showing that two different S-M adsorption sites were co-existed in Y(III)-Y. For Cu(I)-Y(III)-Y, it is interesting to find that in addition to all the above mentioned peaks (339, 378, 450 and 509 °C) that appeared in Cu(I)-Y and Y(III)-Y, a new weight loss deformation peak at 533 °C (Fig. 4f) was also found. The corresponding temperatures of these former three peaks were the same with those found for Cu(I)-Y and Y(III)-Y. Therefore, one can conclude that Cu(I)-Y(III)-Y possessed

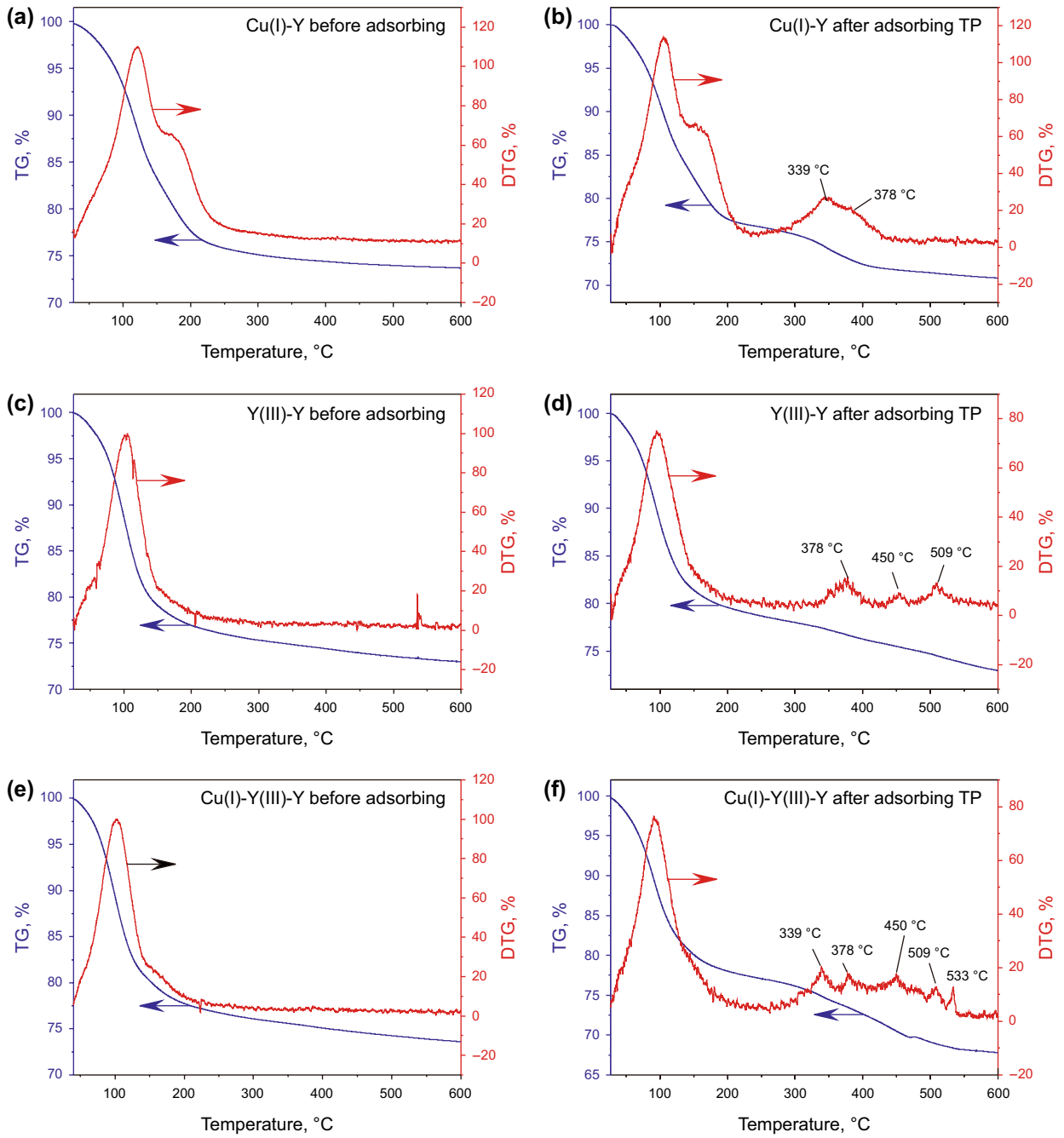

Fig. 4 TG and DTA curves of Cu(I)-Y, Y(III)-Y and Cu(I)-Y(III)-Y before and after adsorbing TP

all the active sites existing in both Cu(I)-Y and Y(III)-Y (Scheme 1). The new peak located at 533 °C, which possessed the highest temperature among these peaks, indicated the existence of relatively stronger S-M interaction sites in Cu(I)-Y(III)-Y. As this peak was not found for Cu(I)-Y and Y(III)-Y, it might be caused by the synergistic effect between Cu(I) and Y(III). The excellent selective adsorption performance of Cu(I)-Y(III)-Y in presence of xylene isomers (Sect. 3.2.2) can be explained by the new stronger S-M interaction sites.

4.1.2 Analysis of ADS mechanism

To analyze the mechanism of ADS and the effects of xylenes on ADS, FT-IR spectra of the Cu(I)-Y, Cu(I)-Y(III)-Y and Y(III)-Y adsorbents before and after adsorbing model gasolines M1, M3, M4 and M5 were recorded, and the results are shown in Fig. 5. Compared with the fresh adsorbents (Fig. 5a), the new peaks appeared at 2858 and 2930 cm^{-1} for all the adsorbents after adsorbing model gasolines M1, M3, M4 and M5 (Fig. 5b–e). This demonstrates that some of the adsorbed TP underwent the opening of their thiophenic ring during adsorption processes (Hernández-Maldonado and Yang 2003). For all the adsorbents, the new peak at 1394 cm^{-1}, which was 12 cm^{-1} lower compared with that of weakly adsorbed TP on SiO_2 (Yi et al. 2014), can be attributed to TP molecules interacting with the extra framework cations by π-complexation interactions (Yi et al. 2014; Wang et al. 2020). For Cu(I)-Y(III)-Y and Y(III)-Y, the new band at 1452 cm^{-1}, which can be attributed to a red shift of vibration of $\nu(C{=}C)_{sym}$ (Song et al. 2014), can be assigned to TP molecules coordinated with Y(III) sites via the S atom (Yi et al. 2014). And the new peak at 1452 cm^{-1} can also be assigned to the protonation of TP on the Brönsted acid sites (Sara et al. 2002; Zu et al. 2019a), which is in agreement with the TG-DTG analysis. It should be noted that the peak intensity at 1452 cm^{-1} was little affected by addition of xylenes (Shi et al. 2013). This demonstrates S-M interaction and protonation (Scheme 2) play an important role in competitive ADS in presence of xylenes (Lee and Valla 2017). Moreover, the intensity of the peaks at 2930 and 2858 cm^{-1} decreased after adsorbing xylenes (Gabruś et al. 2015). These phenomenons demonstrated that xylenes had a competitive effect on TP adsorption mainly via π-complexation interaction due to the similarity in molecular structures (Shi et al. 2012).

In addition to the four new peaks mentioned above, the adsorbents after adsorbing the model gasoline-containing xylenes (Fig. 5c–e) showed a new infrared band at 1497 cm^{-1}, which can be attributed to the vibrations of the benzene ring of adsorbed xylenes (Li et al. 2009; Qin et al. 2014a). The differences between the adsorbents after absorbing different xylene isomers were detected in the range of 600–900 cm^{-1} (Fig. 5c–e), which could be ascribed to the characteristic adsorption peaks of adsorbed m-xylene, o-xylene and p-xylene in the fingerprint region, respectively.

4.2 Computer simulations

In an attempt to explain the reason for the observed selectivity trend in our studies, computer-aided orbital calculations of sulfur compounds and xylene isomers have been carried out, and the results are listed in Table 3. According to the chemical bond order data listed in Table 3, o-xylene possessed the lowest bond order value of 1.166, which indicated that the C–C chemical bonds in o-xylene were weak among its isomers. Therefore, o-xylene possessed the strongest ability for electronic delocalization, which means that o-xylene is the most easily adsorbed onto the adsorbents via π-complexation among its isomers (Velu et al. 2003). Therefore, the o-xylene might exhibit the strongest effect on ADS. The bond order of xylenes increased in the order of o-xylene (1.166) < m-xylene (1.441) < p-xylene (1.443). This result is in agreement with the result obtained in Sect. 3.2, which showed that the effect of xylenes on ADS of BT and TP

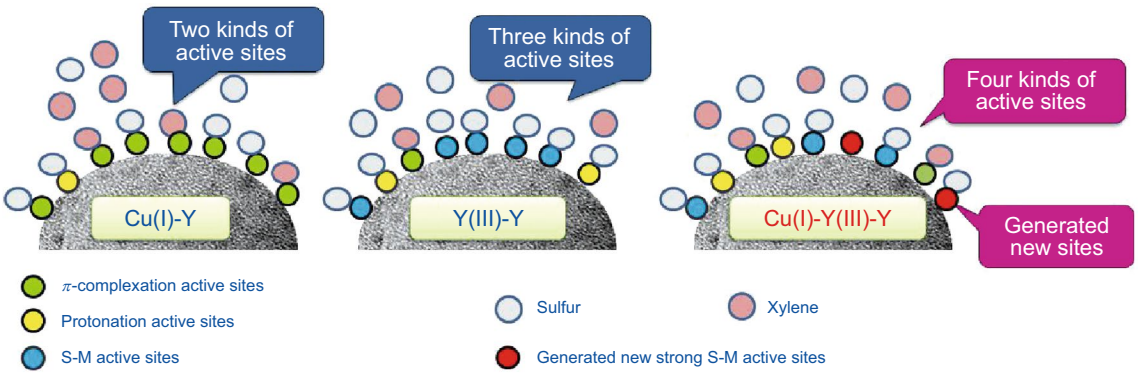

Scheme 1 The active ADS sites on Cu(I)-Y, Y(III)-Y and Cu(I)-Y(III)-Y

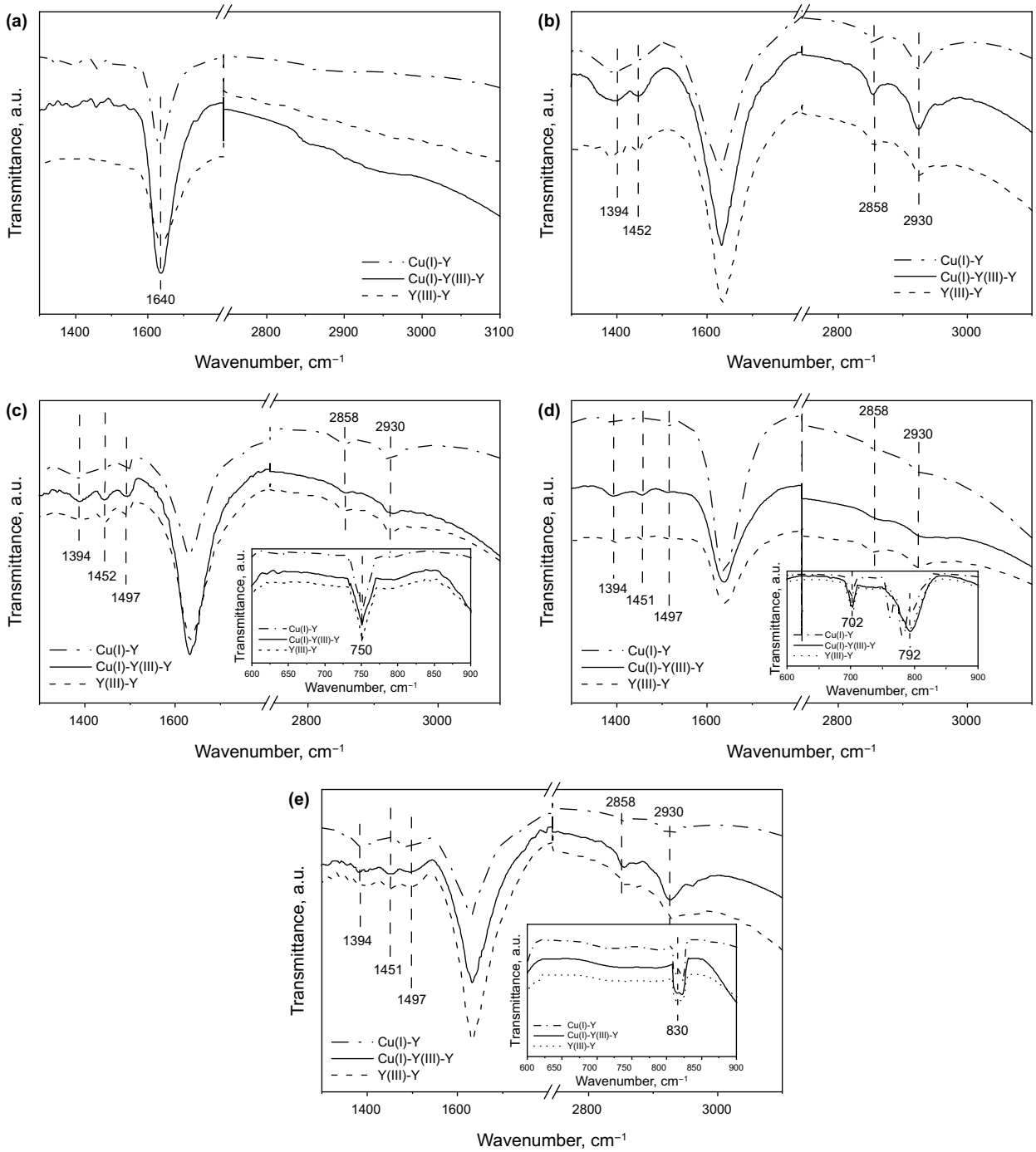

Fig. 5 FT-IR spectra of Cu(I)-Y, Y(III)-Y and Cu(I)-Y(III)-Y before and after adsorbing different model gasolines: before absorption (**a**), after adsorbing M1 (**b**), M3 (**c**), M4 (**d**) and M5 (**e**)

decreased in the order of o-xylene > m-xylene > p-xylene (see Table S2 and Fig. 3).

The electron density (Velu et al. 2003) and adsorption energy (Wang et al. 2012) obtained from references are also listed in Table 3. It can be seen that the electron density and adsorption energy were both in the order of BT (1.769, 22.9 kcal mol^{-1}) > TP (5.696, 21.4 kcal mol^{-1}). The BT, which possessed the higher electron density, leads to the stronger linkage with metal sites via the S-M interaction. While the higher adsorption energy of BT means strong interaction between sulfur and zeolites. Therefore, the higher ADS selectivity to BT than TP on the Cu(I)-Y(III)-Y could

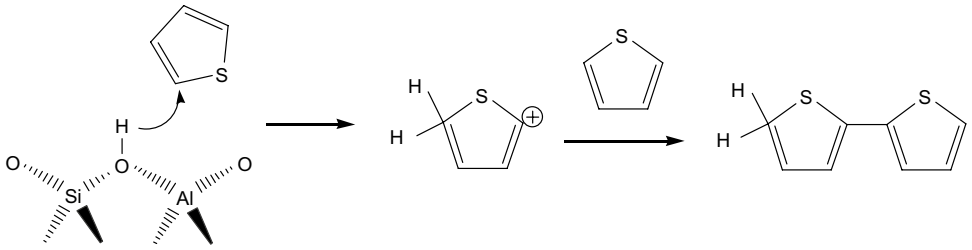

Scheme 2 The mechanism of TP protonation on Brönsted acid sites

Table 3 Electron density of sulfur atom and bond order of the largest bonds of xylene iosmers obtained from computer-simulated molecular orbital calculations

Compounds	Bond order[a]	Electron density on S atom (no. ofelectrons per S atom) (Velu et al. 2003)	Adsorption energy[b], kcal mol^{-1} (Wang et al. 2012)
TP	1.689	5.696	21.4
BT	1.769	1.769	22.9
o-xylene	1.166	–	
m-xylene	1.441	–	
p-xylene	1.443	–	

[a]Bond order of the C–C bond with largest bond order value in the given molecule. For all the molecules, it is between C2 and C3 carbons

[b]Adsorption energy calculated using molecular orbital theory for adsorption of BT and TP onto CuY

be explained by the higher adsorption energy and electron density of BT compared with those of TP.

5 Conclusions

The Y(III) and Cu(II) bimetal-exchanged NaY zeolite with a desirable adsorption selectivity was prepared by ion-exchange method, and then the Cu(I)-Y(III)-Y was obtained by reduction. The TG-DTG analysis demonstrated that a new strong S-M interaction active site was formed on Cu(I)-Y(III)-Y, which might be caused by the synergistic effect between Cu(I) and Y(III). The ADS performances of Y(III)-Y with and without aromatic competitors were both higher than that of most reported CeY. The Y(III)-based Cu(I)-Y(III)-Y demonstrated the higher breakthrough loading than that of reported Ce(III)/Ce(IV)-based transition metal Y zeolites, showing that the Y(III) ions play a promoting role in improving the selective ADS. The Cu(I)-Y(III)-Y zeolite bind sulfur compounds via π-complexation, direct coordination (S-M) interactions and protonation. It possessed the highest breakthrough loading for the model oils containing xylene isomers, and the breakthrough loading decreased in the order of Cu(I)-Y(III)-Y > Y(III)-Y > Cu(I)-Y, which indicated that Cu(I)-Y(III)-Y is a kind of promising adsorbent. The effects of the xylene isomers on ADS onto zeolites exhibited the same trend with the bond order of xylenes, which was in the order of o-xylene > m-xylene > p-xylene.

Acknowledegments The authors acknowledge the financial supports from the National Natural Science Foundation of China (81172204).

Availability of data and material All the data and materials in this manuscript are transparent.

Compliance with ethical standards

Conflict of interest The author(s) declare that they have no competing interests.

Code availability Not applicable.

References

Bhandari VM, Ko CH, Park JG, Han SS, Cho SH, Kim JN. Desulfurization of diesel using ion-exchanged zeolites. Chem Eng Sci. 2006;61:2599–608. https://doi.org/10.1016/j.ces.2005.11.015.

Bondarenka V, Grebinskij S, Kaciulis S, Mattogno G, Mickevicius S, Tvardauskas H, Volkov V, Zakharova G. XPS study of vanadium-yttrium hydrates. J Electron Spectrosc Relat Phenom. 2001;120:131–5. https://doi.org/10.1016/S0368-2048(01)00312-7.

Emeis CAJ. Determination of integrated molar extinction coefficients for infrared absorption bands of pyridine adsorbed on solid acid catalysts. J Catal. 1993;141:347–54. https://doi.org/10.1002/chin.199338056.

Gabruś E, Nastaj J, Tabero P, Aleksandrzak T. Experimental studies on 3A and 4A zeolite molecular sieves regeneration in TSA process: aliphatic alcohols dewatering-water desorption. Chem Eng J. 2015;259:232–42. https://doi.org/10.1016/j.cej.2014.07.108.

Gong Y, Dou T, Kang S, Li Q, Hu Y. Deep desulfurization of gasoline using ion-exchange zeolites: Cu(I)- and Ag(I)-beta. Fuel Process Technol. 2009;90:122–9. https://doi.org/10.1016/j.fuproc.2008.08.003.

Gupta P, Paul S. Solid acids: green alternatives for acid catalysis. Catal Today. 2014;236:153–70. https://doi.org/10.1016/j.cattod.2014.04.010.

Hernández-Maldonado AJ, Yang FH, Qi G, Yang RT. Desulfurization of transportation fuels by π-complexation sorbents: Cu(I)-, Ni(II)-, and Zn(II)-zeolites. Appl Catal B. 2005;56:111–26. https://doi.org/10.1016/j.apcatb.2004.06.023.

Hernández-Maldonado AJ, Yang RT. Desulfurization of liquid fuels by adsorption via π-complexation with Cu(I)-Y and Ag-Y zeolites. Ind Eng Chem Res. 2003;42:123–9. https://doi.org/10.1021/ie020728j.

Isoda T, Takase Y, Kusakabe K, Morooka S. Changes in desulfurization reactivity of 4,6-dimethyldibenzothiophene by skeletal isomerization using a Ni-supported Y-type zeolite. Energy Fuel. 2000;14:585–90. https://doi.org/10.1021/ef990018z.

Kim JG, Kompany T, Ryoo RT, Fraissard J. ^{129}Xe N.M.R. of Y^{3+}-, La^{3+}-, and Ce^{3+}-exchanged X zeolites. Zeolites. 1994;14:427–32. https://doi.org/10.1016/0144-2449(94)90168-6.

Kolev I, Mavrodinova V, Alexieva G, Strashilov V. Pore volume probing of boron-modified MCM-22 zeolite by quartz crystal microbalance assisted study of o- and p-xylene adsorption. Sensors Actuators B-Chem. 2010;149:389–94. https://doi.org/10.1016/j.snb.2010.06.044.

Lee KX, Valla JA. Investigation of metal-exchanged mesoporous Y zeolites for the adsorptive desulfurization of liquid fuels. Appl Catal B. 2017;201:359–69. https://doi.org/10.1016/j.apcatb.2016.08.018.

Li JR, Yang Z, Li SW, Jin QP, Zhao JS. Review on oxidative desulfurization of fuel by supported heteropolyacid catalysts. J Ind Eng Chem. 2020;82:1–16. https://doi.org/10.1016/j.jiec.2019.10.020.

Li HZ, Dong LX, Zhao L, Cao LY, Gao JS, Xu CM. Enhanced adsorption desulfurization performance over mesoporous ZSM-5 by alkali treatment. Ind Eng Chem Res. 2017;56:3813–21. https://doi.org/10.1021/acs.iecr.6b05053.

Li X, Zhang X, Lei L. Preparation of CuNaY zeolites with microwave irradiation and their application for removing thiophene from model fuel. Sep Purif Technol. 2009;64:326–31. https://doi.org/10.1016/j.seppur.2008.10.016.

Liao J, Bao W, Chang L. An approach to study the desulfurization mechanism and the competitive behavior from aromatics: a case study on CeY zeolite. Fuel Process Technol. 2015;140:104–12. https://doi.org/10.1016/j.fuproc.2015.08.036.

Liu X, Wang J, Li Q, Jiang S, Zhang H, Ji SJ. Synthesis of rare earth metal-organic frameworks (Ln-MOFs) and their properties of adsorption desulfurization. J Rare Earth. 2014;32:189–94. https://doi.org/10.1016/S1002-0721(14)60050-8.

Mo Z, Qin Y, Zu Y, Wang H, Zhang X, Song L. Effect of content of cerium ion on Brönsted-Acid-Catalyzed reaction of thiophene over CeY zeolite studied by In Situ FT-IR spectroscopy. Chem Sel. 2019;4(44):13034–44. https://doi.org/10.1002/slct.201903194.

Moulder JF, Stickle WF, Sobol PE, Bomben KD. Handbook of X-ray photoelectron spectroscopy. Phys Electron Eden Praire. 1995;2553:316–28.

Oliveir MLM, Miranda AAL, Barboa CMBM, Cavalcante CL, Azevedo DCS, Rodriguez-Castellon E. Adsorption of thiophene and toluene on NaY zeolites exchanged with Ag(I), Ni(II) and Zn(II). Fuel. 2009;88:1885–92. https://doi.org/10.1016/j.fuel.2009.04.011.

Qin Y, Mo Z, Yu W, Dong S, Duan L, Gao X, Song L. Adsorption behaviors of thiophene, benzene, and cyclohexene on FAU zeolites: comparison of CeY obtained by liquid-, and solid-state ion exchange. Appl Surf Sci. 2014a;292:5–15. https://doi.org/10.1016/j.apsusc.2013.11.036.

Qin YC, Gao XH, Duan LH, Fan YC, Yu WG, Zang HT, Song LJ. Effects on adsorption desulfurization of CeY zeolites: acid catalysis and competitive adsorption. Acta Phys Chim Sin. 2014b;30:544–50. https://doi.org/10.3866/PKU.WHXB201401021.

Sara YY, Garcia-Martinez J, Li W, Meitzner GD, Iglesia E. Kinetic, infrared, and X-ray absorption studies of adsorption, desorption, and reactions of thiophene on H-ZSM5 and Co/H-ZSM5. Phys Chem Chem Phys. 2002;4:1241–51. https://doi.org/10.1039/b108640p.

Shi Y, Zhang W, Zhang H, Tian F, Jia C, Chen Y. Effect of cyclohexene on thiophene adsorption over NaY and LaNaY zeolites. Fuel Process Technol. 2013;110:24–32. https://doi.org/10.1016/j.fuproc.2013.01.008.

Shi YC, Yang XJ, Tian FP, Jia CY, Chen YY. Effects of toluene on thiophene adsorption over NaY and Ce(IV)Y zeolites. J Nat Gas Chem. 2012;21:421–5. https://doi.org/10.1016/S1003-9953(11)60385-X.

Song H, Cui XH, Song HL, Gao HJ, Li F. Characteristic and adsorption desulfurization performance of Ag-Ce bimetal ion-exchanged Y zeolite. Ind Eng Chem Res. 2014;53:14552–7. https://doi.org/10.1021/ie404362f.

Song H, Gao HJ, Song HL, Yang G, Li XJ. Effects of Si/Al ratio on adsorptive removal of thiophene and benzothiophene over ion-exchanged AgCeY zeolites. Ind Eng Chem Res. 2016;55:3813–22. https://doi.org/10.1021/acs.iecr.5b04609.

Song H, Wan X, Dai M, Zhang JJ, Li F, Song HL. Deep desulfurization of model gasoline by selective adsorption over Cu-Ce bimetal ion-exchanged Y zeolite. Fuel Process Technol. 2013;116:52–62. https://doi.org/10.1016/j.fuproc.2013.04.017.

Song H, Wang N, Song HL, Li F. La-Ni modified $S_2O_8^{2-}/ZrO_2$–Al_2O_3 catalyst in n-pentane hydroisomerization. Catal Commun. 2015;59:61–4. https://doi.org/10.1016/j.catcom.2014.09.03.

Subhan F, Aslam S, Yan ZF, Zhen L, Ahmad A. Ammonia assisted functionalization of cuprous oxide within confined spaces of SBA-15 for adsorptive desulfurization. Chem Eng J. 2018a;339:557–65. https://doi.org/10.1016/j.cej.2018.01.146.

Subhan F, Aslam S, Yan Z, Naeem M, Ullah R, Etim UJ. Size regulation and dispersion of ceria using confined spaces for adsorptive desulfurization. Chem Eng J. 2018b;348:319–26. https://doi.org/10.1016/j.cej.2018.04.213.

Tarafdar A, Panda AB, Pramani P. Synthesis of ZrO_2-SiO_2 mesocomposite with high ZrO_2 content via a novel sol-gel method.

Microporous Mesoporous Mater. 2005;84:223–8. https://doi.org/10.1016/j.micromeso.2005.05.014.

Thomas JK, Gunda K, Rehbein P, Flora TT. Flow calorimetry and adsorption study of dibenzothiophene, quinoline and naphthalene over modified Y zeolites. Appl Catal B. 2010;94:225–33. https://doi.org/10.1016/j.apcatb.2009.11.012.

Velu S, Ma X, Song C. Selective adsorption for removing sulfur from jet fuel over zeolite-based adsorbents. Ind Eng Chem Res. 2003;43:5293–304. https://doi.org/10.1021/ie020995p.

Wang H, Song L, Jiang H, Xu J, Jin L, Zhang X, Sun Z. Effects of olefin on adsorptive desulfurization of gasoline over Ce(IV)Y zeolites. Fuel Process Technol. 2009;90:835–8.

Wang H, Xu R, Jin Y, Zhang R. Zeolite structure effects on Cu active center, SCR performance and stability of Cu-zeolite catalysts. Catal Today. 2019;327:295–307. https://doi.org/10.1016/j.cattod.2018.04.035.

Wang HG, Jiang H, Xu J, Sun ZL, Zhang XT, Zhu HL, Song LJ. Effects of benzene and 1-octene on desulfurization by selective adsorption with Ce(IV)Y. Acta Phys Chim Sin. 2008;24:1714–8. https://doi.org/10.3866/PKU.WHXB20080933 **(in Chinese)**.

Wang LF, Baode S, Yang FH, Yang RT. Effects of aromatics on desulfurization of liquid fuel by π-complexation and carbon adsorbents. Chem Eng Sci. 2012;73:208–17. https://doi.org/10.1016/j.ces.2012.01.056.

Wang PZ, Zhang JY, Han CY, Yang CH, Li CY. Effect of modification methods on the surface properties and *n*-butane isomerization performance of La/Ni-promoted SO_4^{2-}/ZrO_2–Al_2O_3. Appl Surf Sci. 2016;378:489–95. https://doi.org/10.1016/j.apsusc.2016.04.043.

Wang SH, Zu Y, Qin YC, Zhang XT, Song LJ. Fabrication of effective desulfurization species active sites in the CeY zeolites and the adsorption desulfurization mechanisms. J Fuel Chem Technol. 2020;48:52–62. https://doi.org/10.1016/S1872-5813(20)30003-7.

Yi DZ, Huang H, Meng X, Shi L. Adsorption-desorption behavior and mechanism of dimethyl disulfide in liquid hydrocarbon streams on modified Y zeolites. Appl Catal B. 2014;148–149:377–86. https://doi.org/10.1016/j.apcatb.2013.11.027.

Zu Y, Hui Y, Qin Y, Zhang L, Liu H, Zhang X, Guo Z, Song L, Gao X. Facile fabrication of effective Cerium(III) hydroxylated species as adsorption active sites in CeY zeolite adsorbents towards ultra-deep desulfurization. Chem Eng J. 2019a;375:122014.

Zu Y, Zhang C, Qin YC, Zhang XT, Zhang L, Liu HH, Gao XH, Song LJ. Ultra-deep adsorptive removal of thiophenic sulfur compounds from FCC gasoline over the specific active sites of CeHY zeolite. J Energy Chem. 2019b;39:256–67. https://doi.org/10.1016/j.jechem.2019.04.010.

Zu Y, Guo ZS, Zheng J, Hui Y, Wang SH, Qin YC, Zhang L, Liu HH, Gao XH, Song LJ. Investigation of Cu(I)-Y zeolites with different Cu/Al ratios towards the ultra-deep adsorption desulfurization: discrimination and role of the specific adsorption active sites. Chem Eng J. 2020;380:122319. https://doi.org/10.1016/j.cej.2019.122319.